Contents

1 Introduction

Carbon is unique among the elements in its ability to form strong chemical bonds with a variety of coordination numbers, including two (e.g. linear chains or carbyne phase), three (e.g. graphite) and four (e.g. diamond). Combining strong bonds with light mass and high melting point, condensed carbon phases have many unique properties that make them technologically important as well as scientifically fascinating.

Reducing the size of semiconductors to the nanometer scale changes the physical properties of the materials in a fundamental way. For example, semiconductor nanoclusters exhibit an increased optical gap and narrower emission spectra when compared with bulk values [1, 2, 3, 4]. In addition, the physical and chemical properties of semiconductor nanoclusters are greatly influenced by surface reconstruction and passivation [5, 6]. Quantum confinement effects have been intensively studied theoretically and experimentally over the last decade [7, 8, 9, 10]. These studies suggest that these nanostructures may be exploited for specific applications in which they might be integrated within existing semiconductor technologies to create nanoscale optoelectronic devices.

Nanometer sized diamond is a constituent of diverse systems [11], including interstellar dusts and meteorites [12, 13], carbonaceous residues of detonation [14], and diamond-like films. More than a decade ago the presence of nanoparticles in carbonaceous chondrites was reported [12]. While the structural properties of nanodiamonds are basically unexplored, a report on its electronic properties has appeared in the literature [1]. It suggests that reducing the size of diamond may have stronger effects on its optical gap than in the case of Si or Ge. An *ab initio* study of electronic properties of hydrogenated nanodiamonds was recently reported by Galli [15]. This calculation indicates that there are no appreciable quantum confinement effects on the optical gap of nanodiamonds for sizes larger than 1-1.2 nm, which is much smaller than in nanostructures of other semiconductors.

Artifical nanodiamond is produced by detonation of diamond containing materials and subsequently by chemical purification. Nowdays nanodiamond has many applications, such as: electrochemical and chemical deposition, metal matrix composite with aluminium and copper, an additive for PTFE (Teflon), polishing pastes and suspensions, an additive to rubber, abrasive tools, lubrificating oils, greases and coolants, systems of magnetic recording, intermetallic on the basis of copper, zin and tin [16]. Many other applications of this material may be discovered.

The purpose of the present study is to investigate the electronic properties of nanodiamond clusters with a size up to 2 nm, nanodiamond wires with a diameter of their cross section up to 1-2 nm and nanodiamond layers with a thickness of a few nm by *ab initio* molecular dynamics and by tight-binding molecular dynamics. In order to exclude the surface reconstruction effects or the need to terminate the dangling bonds with hydrogen the clusters and the layers will be surrounded by amorphous carbon phase. This is one of the forms of nanodiamonds which was found in nature. To the best of our knowledge this type of geometry has not been previously applied in this context.

Simulations of amorphous carbon and the phase transformations of carbon at the boundary between crystalline diamond and amorphous carbon $ta-C$ at very high temperatures were carried out in the MSc thesis of Anastassia Sorkin by means of tight-binding molecular dynamics techniques [19]. Following the computational techniques developed in this research project the samples of nanodiamond clusters and layers of different sizes passivated by amorphous carbon will be prepared by different conditions (temperature and cooling rate). The structural and electronic properties of each sample will be studied. These results can help in interpreting experimental data for diamond nanoclusters [1]. Such an investigation of the factors which influence quantum confinement effects in nanodiamonds is a crucial step toward the utilization of these materials for new technologies.

2 Background

2.1 Diamond and graphite properties

The electronic configuration of carbon is $1s^2 2s^2 2p^2$, i.e. four valence electrons spread in the s and p orbitals. In order to create covalent bonds in diamond, the s orbital mixes with the three p orbitals to form sp^3 hybridization. The four valence electrons are thus equally distributed among the sp^3 orbitals, while each orbital points to one of the four corners of a tetrahedron. The tetrahedral structure, together with the highly directed charge density, give strength and stability to the bonds. Consequently, all the bonds in diamond are of the same length (1.54 $\mathring{A}$), with the same bond angle (109.47^o). Diamond is a wide gap semiconductor (insulator) and is very hard, and has a melting temperature of 4500 K.

In the graphite crystal, the s orbital mixes with two p orbitals only, and each of the new three sp^2 orbitals points to one of the three vertices of a triangle which lies in the $x-y$ plane (for instance). Three electrons occupy these orbitals and one electron stays in the p_z orbital which is directed perpendicular to the $x-y$ plane. Hence, the carbon atoms are bonded by three σ bonds (the charge density lies between two atoms) and one π bond (the charge density is concentrated above and under the $x-y$ plane, perpendicular to the atomic bond). Since there is no preference as to which atom the p_z-electron should bond to, the π bond formed with all three neighbors is weaker than the σ bonds, and this electron is more free to move and contributes to conduction. Furthermore, the π bond stabilizes the structure and "locks" it in the plane. The whole crystal is made of sheets of hexagon, with carbon atoms in corners. These sheets are held together by weak Van der Waals forces, separated by a distance of 3.40 Å. This gives softness to the structure.

The stable bonding configuration of carbon at NTP is graphite, as shown in figure 1, with an energy difference between the graphite and the diamond ground state of ≈ 0.02 eV per atom. Due to the high energetic barrier between the two phases of carbon, the transition from diamond to the stablest phase of carbon, graphite, at normal conditions is very slow. This transition can also occurs more rapidly, when diamond is exposed, for example, to ion bombardment or high temperature [19].

Bridging between these two allotropes of carbon lie a whole variety of carbon materials which include, among others, amorphous sp^2 bonded carbon (such as thermally evaporated carbon), micropolycrystalline sp^2 bonded graphite (such as glassy carbon),

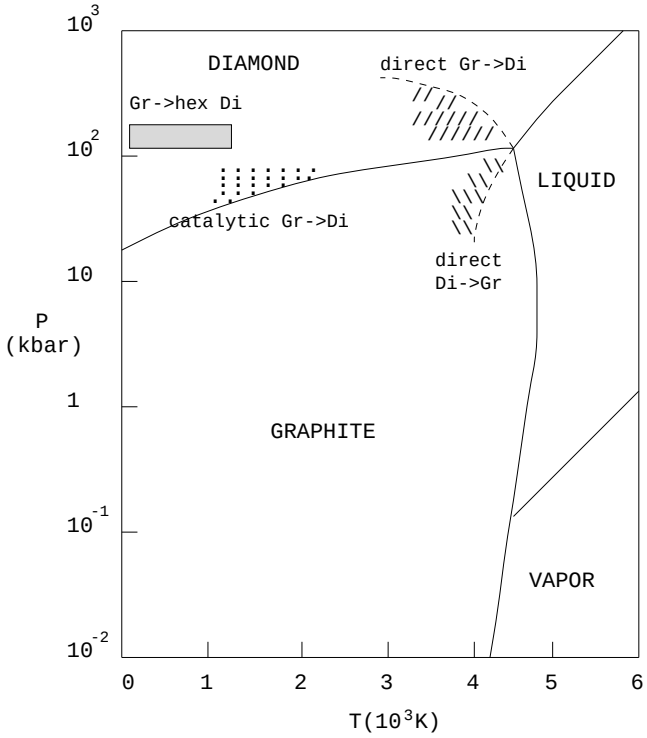

Figure 1: P, T phase diagram of carbon reproduced from ref. [18]

nanodiamond films, and amorphous sp^3 bonded carbon (sometimes referred to as amorphous diamond), which is structurally analogous to amorphous Si and is formed during low energy carbon ions deposition. Another polymorphic form of carbon was discovered in 1985. It exists in discrete molecular form, and consists of a hollow spherical cluster of carbon atoms. Each molecule is composed of groups of sixty and more carbon atoms that are bonded to one another form both hexagons and pentagons geometrical configuration. The material composed of C_{60} is known as buckminsterfullerene, named in honor of R. Buckminster Fuller, who invented the geodesic dome. In the solid state, the C_{60} units form a crystalline structure and pack together in a face-centered cubic array. Molecular shapes other than the ball clusters recently have been discovered: these include nanoscale tubular and polyhedral structures. It is anticipated that, with further developments, the fullerenes will become technologically important materials [20]. Their possible applications in high-temperature lubricants, microfilters, more efficient semiconductors, and manufacturing processes [21].

Nanodiamond, the leading nanomaterial, is ball-shaped with the particle diameter up to 15 nanometers. It is hard, chemically stable, abrasion-resistant, super corrosion-

resistant and has high heat conductivity and refractory. It also has good biological compatibility and cold electron emission properties. The production process of nanodiamonds consists of two stages. The first one is instantaneous detonation of mixed high explosives forms ultradispersive diamond-graphite powder (also known as diamond blend or DB), a black powder containing 40-60 % of pure diamond. The second stage is the product is a chemical purification of DB generated pure nanodiamond (also known as Ultradispersive detonational diamond - UDD), a grey powder containing up to 99,5 % of pure diamond. Diamonds just 3-5 nm in diameter have recently been recovered from carbonaceous residues of detonations. They have also been found in meteorites and interstellar stardust.

Nanodiamond films can be grown by different deposition techniques such as dc assisted plasma chemical vapor deposition (CVD) from a methane-hydrogen mixture [22, 23]. The criteria of quality of the nanodiamond films include low-contents of nondiamond phases, nano-sizes crystallites, uniform nanocrystallinity throughout thick films and random grain orientation.

2.2 Quantum confinement

Quantum confinement results in a shift in energy levels when the material sampled is of sufficiently small size - typically 10 nanometers or less. This leads to change of electronic and optical properties of nanostructures. The bandgap increases as the size of the nanostructure decreases. Specifically, the phenomenon results from electrons and holes being squeezed into a dimension that approaches a critical quantum measurement, called the exciton Bohr raduis.

The first experimental evidence of the quantum confinement effects in clusters came from crystalline CuCl clusters grown in silicate glasses [2]. Spectroscopic studies on these clusters clearly indicated an up to 0.1 eV blueshift of the absorption spectrum relative to the bulk. In the case of CdS clusters, the absorption threshold is observed to blueshift by up to 1eV or more as the cluster size is decreased [3]. When the size of the cluster is smaller, its band gap is larger, consequently the first absorption peak is shifted closer to the blue.

A recent study [1] of the X-ray absorption spectra in nanodiamond thin films showed that the exciton state and conduction band edge are shifted to higher energies with decrease of the grain size especially when the crystallite radius is smaller than $\sim$1.8

nm. The conduction band of nanodiamonds with radius $R > 1.8$ nm, when the crystallite contains more than 4300 C atoms, remain more or less bulklike.

Although the basic principles governing the relationship between cluster size and the band gap appears to be understood, theoretical simulations have not been able to predict the observed blueshift quantitatively. The effects of other factors, such as the physical shape and crystal structure, have not yet been understood.

2.3 Effective-mass model

Brus and co-workers [7, 24] gave a very elegant analysis of the observed blueshift utilizing a particle in a sphere and the effective mass model. They retained the effective mass approximation for the kinetic energy of the electron-hole pair and used classical electrostatics to determine the potential energy of interaction of the electron and the hole with each other and the with the surface.

The onset of absorption of light by semiconductor materials is accompanied by the creation of a bound electron-hole pair called an exciton. The effective mass model (EMM) suggests that the effects of the interaction of the electron and the hole with the periodic potential of the lattice is such that m_e and m_h are usually less than the free-electron mass m_0. Batson and Heath [25] based on the effective mass model predicted that the shift of conduction band edge of spherical clusters follows the equation

$$E = E_{re} + \frac{\hbar^2}{2m^*}\left(\frac{\pi}{R}\right)^2,$$

where E_{re} is the bulk reference energy and m^* and R are the electron effective mass in the nanocrystal and the radius of the nanocrystal respectively. Chang *et al* [1] estimated m^* for their largest nanodiamonds (more than 4300 carbon atoms) to be 0.1 ± 0.02 m_e, which is reasonably close to that of the bulk diamond, 0.2-0.25 m_e [26].

The calculations based on this model have yielded the blueshift of the absorption spectrum in reasonable agreement with experiment for large clusters [7]. However there are deficiencies of the EMM, which contribute to the failure of the model to quantitatively predict the quantum confinement effects in small clusters.

2.4 Previous computer simulations of the quantum confinement effects

During the last few years, many investigations of the quantum confinement effects in semiconductor materials were carried out by means of computer simulations. In most of them *ab initio* and tight-binding molecular dynamics methods (see sections 4,5) which allow the study of the electronic structure of materials were used.

Ab initio molecular dynamics treats the motion of the atomic core classically, while the electron wave functions are represented in terms of a large basis set of plane waves, keeping the energy of the whole system close to a minimum with respect to the wave function. Such a many-body problem remains formidable even for the most powerful computers, therefore further simplifications are needed to allow an efficient calculation of a system consisting of many atoms. This technique with the *local-density approximation* of *density functional theory* (see below) was used by K. E. Andersen *et al* [9] to investigate the energy levels in CdSe nanocrystallites containing 17-34 atoms. The authors confirmed that the lowest unoccupied energy state and the highest occupied energy state are strongly affected by quantum confinement.

Small CdS and ZnS crystallite (20-2500 atoms) were investigated by a tight-binding empirical approximation by Lippens and Lanoo [27]. Here the electron wave functions are expanded in terms of basis set of valence electrons wave functions, rather than plane waves, controlling the attractive part of the potential, while the repulsive part is treated empirically. In this study a simple model of the crystal of symmetrical shape without dangling bonds is used. The position of the exciton peak and band gap were determined and compared with calculation based on effective-mass approximation. It has been shown that the effective-mass calculation strongly overestimates the band gap for the smallest size of the crystallites.

The band structure and spectral shift of CdS, CdSe, CdTe, AlP, GaP, GaAs and InP semiconductor nanoclusters were calculated using an empirical pseudopotential by Rama Krishna *et al* [8]. The authors replaced the exact crystal-field potential experienced by the valence electrons to an effective potential (pseudopotential). For CdS clusters the calculation had yielded exciton energies in excellent agreement with experiment over a wide range of cluster sizes. The authors also found that not only the size of nanoclusters but the shape, crystal structure and lattice constant of the unit cell all have significant

effect on the exciton energies.

The discovery of photoluminescence (PL) in Si and Ge nanocrystals [28, 4] stimulated great interest in these indirect-gap semiconductors crystallites in the last decade. The empirical pseudopotentials method was used to study the electronic and optical properties of Si cubic prism with edge of the cube d ranging from 10 Å to 30 Å [29]. It is found that the energy gap vary with equivalent diameter d as $d^{-1.37}$. Yeh *et al* [30] used another pseudopotential for [001]Si quantum wires with square cross sections ranging from 7.7×7.7 to 26.9×26.9 Å with a free surface but without hydrogen and wires with hydrogen chemisorption on the surface. They found that in both cases the band gap increases as the wire diameter decreases due to quantum confinement, however hydrogen chemisorption acts to reduce the gap.

Niquet with co-workers [31] proposed a new parameterization for tight-binding model: the orthogonal third-nearest-neighbor sp^3 TB model, designed to give accurate results in the calculation of confined edge states in semiconductors. They applied it to silicon nanostructures (films, wires and dots) with large range of sizes (1-12 nm) with various shapes and orientations. Surface dangling bonds were saturated with hydrogen atoms. They found that for spherical and cubic Si dots the curves of size dependence of highest occupied state and lowest unoccupied state in the entire size range are fitted by expression K/d^2, were d is the characteristic dimension of the nanostructure and K is an adjustable constant. They repeated their calculation with Ge nanocrystals [32] up to 12 nm (∼50000 atoms) with dangling bonds passivated by hydrogen atoms. In the case of Ge the results for a gap disagreed with experimental photoluminescence data. This means that the PL in Ge cannot be explained by a simple quantum confinement model. Finally the authors used their model to investigate the quantum confinement effects in amorphous silicon layers [33] with thickness below 3 nm. The calculated confinement effect of the amorphous slabs remains noticeable but weaker than in crystalline Si slabs.

Si and Ge nanoclusters were intensively studied by *ab initio* methods. For example, Öğut and Chelikowsky [10] found the exciton energy and band gap of hydrogen-passivated spherical Si clusters with diameter up to 27.2 Å (∼ 800 Si and H atoms) calculated by an *ab initio* method to be in very good agreement with experiment. The largest radius of hydrogen-passivated Si clusters in *ab initio* study of Delley and Steigmeier [34] was 3 nm (706 Si atoms). Their results suggest that the density-functional band gap scales linearly with d^{-1}, where d is the cluster diameter. The calculated gap covered

the spectral range of experimentally observed photoluminescence peaks for the reported size range of Si nanocrystalline structures. Buda *et al* [35] used an *ab initio* method for electronic-structure calculation of Si wires with diameter up to ~ 1.5 nm. Instead of the indirect gap of crystalline bulk silicon, the band structure of these wires showed a direct gap at $k = 0$. E. Draeger *et al* [5] examined the experimental assumption that optical properties of silicon nanoclusters vary significantly depending on the synthesis technique. Using the *ab initio* method they modeled the $Si_{29}H_6$, $Si_{29}H_{12}$, $Si_{29}H_{22}$, $Si_{29}H_{24}$ and $Si_{30}H_{22}$ nanoclusters with different core structures and different surface passivation which were prepared by relaxation of amorphous clusters at different temperatures with presence of different number of the passivant atoms. They showed that these metastable structures in fact possesses different optical properties, this may be responsible for experimentally observed luminescence. Significant changes which occur in the gap of Si nanoclusters when the surface contains passivants other than hydrogen have been studied by Puzder with co-workers from the same group [6]. They predicted that double bonded groups, like oxygen, strongly affect the optical gap comparing with hydrogen, while other single bonded groups have minimal influence.

In contrast to these numerous computer simulation studies of Si and Ge nanostructures, an interest to carbon nanostructures is still in the early stages. Recently Raty *et al* [15] presented *ab initio* calculations based on density-functional theory (DFT) in order to investigate a quantum confinement effects in hydrogenated nanodiamonds. They detected a rapid decrease of the DFT energy gap from a value of 8.9 eV in methane to 4.3 eV in $C_{87}H_{76}$. The last value is very close to that of the bulk diamond (4.23 eV), obtained using the same method. The computed bulk gap is smaller than the experimental one (5.47 eV), due to well-known error of local density approximations which usually underestimate band gaps in semiconductors and insulators. This indicate that in contrast to Si and Ge where quantum confinement effects persists up to 6-7 nm, in diamond there is no detectable quantum confinement for sizes larger than 1-1.2 nm. In addition the authors predicted a slight influence of surface structure reconstruction by hydrogen atoms on the optical properties.

3 Goal of the research

In the present research project, the structural and electronic properties of small diamond nanostructures (clusters, wires and layers) *embedded in amorphous carbon* will be investigated. The prime interest of this study is quantum confinement effects in nanodiamonds, i.e dependence of electronic properties (width of band gap) on the size of these nanostructures. It is well known that the quantum confinement effects are responsible for photoluminiscence in Si and Ge nanoclusters. The exciton state in nanodiamonds is also shifted to higher energies with decrease of the nanocluster size [1].

Previous computational studies showed that the choice of surface passivant or type of a surface reconstruction influence the band gap of nanoparticles in vacuum [6]. In experiments the formation of nanodiamond clusters can occur in bulk. Lifshitz *et al* [37] proposed a model for diamond nucleation in a dense, amorphous carbon matrix. This process via bias-enhanced nucleation occur in subsurface layers, $\sim$ 1 to 2 nm below the surface. These diamond clusters grow up to several nm (10^4 to 3×10^4 atoms). In the present simulation the clusters, the wires and the layers will be surrounded by an amorphous carbon phase. This type of surface passivation has not been previously used for a quantum confinement investigation of nanoparticles, although this situation is more realistic than nanodiamonds in vacuum. A recent calculation of Fyta *et al* [36] showed that diamonds are stable structures in amorphous carbon matrices with an sp^3 fraction over 60 %.

The diamond nanoclusters, nanowires and nanoslabs surrounded by an amorphous carbon structure will be built using tight-binding molecular dynamics. The diameter of the nanostructures (thickness of nanolayers) will be varied from 3.55 Å to 14.2 Å, i.e from 1 to 4 diamond unit cells, the thickness of the surrounded amorphous phase also will be varied. An outer layer of an initially perfect diamond sample will be heated up to very high temperatures ($\sim$15000- 40000 K). This melting will be followed by a rapid cooling and relaxing. Recent simulations of A. Sorkin [19] showed that by this means this outer envelope should transform to an amorphous phase. In her MSc thesis A. Sorkin investigated transformations of layers of diamond with different thickness (from 14.2 Å to 21.3 Å) sandwiched between layers of frozen diamond (with thickness of 7.1 Å) which occur after heating of the inner layers to a very high temperatures and subsequent quenching. With periodic boundary conditions these structures containing amorphous

carbon layers surrounded by perfect diamond layers can be imagined as a diamond layers of 7.1 Å thickness with a surface passivated by amorphous carbon.

Structures similar to those that will be studied in the present project were prepared by Oren Hershkovitz [38], using the same techniques developed by A. Sorkin for her slab samples. The author built a cubic diamond 7.1×7.1×7.1 Å embedded into a 14.2×14.2×14.2 Å cubic amorphous carbon sample containing 512 atoms. This structure was obtained by heating the outer layers up to 35000 K and then instantly quenching. The $a-C$ envelope consists of 73 % of sp^2 and 27 % of sp^3 coordinated atoms.

In the present research the structures mentioned above will be generated by using the tight-binding molecular dynamics method (the method will be described below in more details). Here, only a reduced basis of four orbitals is used, and an empirical functional describes the repulsive part of the interatomic interaction. This model is less accurate than the *ab initio* but much less computationally expensive. Another advantage of the tight-binding model is its transferability, i.e. the parameters of the model have been chosen to describe successfully different carbon polytypes: diamond, graphite, linear chains, fullerenes [39], as well as a disordered carbon structures like liquid and amorphous carbon phases [40, 41].

The electronic properties of these nanostructures will be then studied as a function of their size and dimension. It is expected that the width of the band gap will be dependent on the ratio of sp^2/sp^3 coordinated atoms in the outer amorphous carbon layers, which in turn depends on the sample preparation conditions. These expectations are supported by the MSc of A. Sorkin, where the ratio of sp^2/sp^3 coordinated atoms in the heated amorphous carbon layers and the band gap of whole sample were very sensitive to heating temperature, cooling rate and thickness of the heated layers. Measurements of the band gap will be carried out by both tight-binding as in the MSc thesis and by *ab initio* techniques. In these methods the electronic density of states is obtained automatically in the process of calculation. *Ab initio* is a more accurate model based on density functional theory (see below). In this model, the local density approximation (LDA) is used for the exchange-correlation interaction. In most calculations, plane waves are used as a basis for the electronic wave functions, and pseudopotentials describe the interaction between the valence electrons and the ionic core. The ionic cores are considered in their ground state at any moment for a particular instantaneous ionic configuration, and the electronic and ionic degrees of freedom can therefore be separated. At each time step the atoms are

considered to be classical particles, which means that Newton's equations can describe their motion.

Periodic boundary conditions will be applied to the problem in all three directions, this means that the unit cell is periodically replicated in all direction to form a macroscopic sample. The duration of calculation will long enough in order to let the structure reach equilibrium. In order to understand the geometry of the obtained structures and the exact structure of the boundary region between diamond and amorphous phase visualization of the heating of the amorphous carbon layers will performed.

4 *Ab initio* molecular dynamics

The term *ab initio* molecular dynamics is used to refer to a class of methods for studying the dynamical motion of atoms, where a huge amount of computational work is spent on solving numerically, as exactly as is required, the entire quantum mechanical electronic structure problem. These methods are extremely accurate but their computational cost is so heavy, that *ab initio* calculations are restricted to a few tens of atoms in short simulation time ($\sim$10 ps). The *ab initio* model based on density functional theory in the local-density approximation was [42] chosen for the present calculations because in spite of its high computational cost, this method gives precise electronic structure information and accurately describes phenomena where quantum mechanical effects are essential.

Prediction of the electronic and geometric structure of a solid requires calculation of the quantum mechanical total energy of the system and subsequent minimization of the energy with respect to the electronic and nuclear coordinates. Because of the large difference in mass between electrons and nuclei, the electrons respond instantaneously to the motion of the nuclei. Thus the nuclei can be treated adiabatically, leading to a separation of electronic and nuclear coordinated in the many body wave function - the Born-Oppenheimer approximation [43]. This approximation reduces the many-body problem to the solution of the electrons in some frozen-in configuration of the nuclei.

4.1 Density functional theory

The most difficult problem in any electronic structure calculation is posed by the need to take into account the effects of the electron-electron interaction. The wave function of a many-electron system must be antisymmetric under exchange of any two electrons because electrons are fermions. The antisymmetry of the wave function produces a spatial separation between electrons that have the same spin and thus reduces the Coulomb energy of the electron system. The reduction in the energy of the electronic system is called the exchange-correlation energy.

Density functional theory was developed by Hohenberg and Kohn [44] in 1964 and Kohn and Sham [45] in 1965. It provides some hope of a simple method for describing the exchange-correlation effects in an electron gas. The Kohn-Sham total energy functional for a set of doubly occupied electronic states, ψ_i, can be written:

$$E([\psi_i]) = 2\sum_i \int \psi_i \left[-\frac{\hbar^2}{2m}\right] \nabla^2 \psi_i \, d^3r + \int V_{ion}(r) n(r) d^3r + \\ + \frac{e^2}{2} \int \frac{n(r) n(r')}{|r - r'|} d^3r \, d^3r' + E_{XC}[n(r)] + E_{ion}([R_I]), \quad (1)$$

where E_{ion} is the Coulomb energy associated with interaction among the nuclei (or ions) at positions $[R_I]$, V_{ion} is the static total electron-ion potential, $n(r)$ is the electronic density, given by

$$n(r) = 2\sum_i |\psi_i(r)|^2 \quad (2)$$

and $E_{XC}[n(r)]$ is the exchange-correlation functional.

Only the minimum value of the Kohn-Sham energy functional has physical meaning. At the minimum, the Kohn-Sham energy functional is equal to the ground-state energy of the system of electrons with the ions in positions $[R_I]$.

It is necessary to determine the set of wave functions ψ_i that minimize the Kohn-Sham energy functional. These are given by the self-consistent solutions to the Kohn-Sham equations:

$$\left[-\frac{\hbar^2}{2m}\nabla^2 + V_{ion} + V_H + V_{XC}\right] \psi_i = \varepsilon_i \, \psi_i(r), \quad (3)$$

where ψ_i is the wave function of electronic state i, ε_i is the Kohn-Sham eigenvalue, and V_H is the Hartree potential of the electrons given by

$$V_H(r) = e^2 \int \frac{n(r')}{|r - r'|} d^3r'. \quad (4)$$

The exchange-correlation potential, V_{XC}, is given formally by the functional derivative

$$V_{XC}(r) = \frac{\delta E_{XC}[n(r)]}{\delta n(r)} \quad (5)$$

The simplest method of describing the exchange-correlation energy of an electronic system is to use the *local density approximation* (LDA) [45], which is almost universally used in total energy pseudopotential calculations. In the local density approximation the exchange-correlation energy of an electronic system is constructed by assuming that the exchange-correlation energy per electron at a point r in the electron gas, $\varepsilon_{XC}(r)$, is equal to the exchange-correlation energy per electron in a homogeneous electron gas that has the same density as the electron gas at point r. Thus

$$E_{XC}[n(r)] = \int \varepsilon_{XC}(r) n(r) d^3r \tag{6}$$

and

$$\frac{\delta E_{XC}[n(r)]}{\delta n(r)} = \frac{\partial [n(r)\, \varepsilon_{XC}(r)]}{\partial n(r)} \tag{7}$$

with

$$\varepsilon_{XC}(r) = \varepsilon_{XC}^{hom}[n(r)]. \tag{8}$$

The local-density approximation assumes that the exchange-correlation energy functional is purely local. Several parametrizations exist for the exchange-correlation energy of a homogeneous electron gas (Wigner [46], Kohn and Sham [45], Hedin and Lundqvist [47], Perdew and Zunger [48]), all of which lead to total-energy results that are very similar.

4.2 Periodic supercell

Bloch's theorem states that in a periodic solid each electronic wave function can be written as the product of a cell-periodic part and a wave-like part [49]

$$\psi_i(r) = \exp[ik * r] f_i(r). \tag{9}$$

The cell-periodic part of the wave function can be expanded using a basis set consisting of a discrete set of plane waves whose plane wave vectors are reprocical lattice vectors of the crystal,

$$f_i(r) = \sum_G c_{i,G} \exp[iG * r], \tag{10}$$

where the reciprocal lattice vectors G are defined by $G * l = 2\pi m$ for all l where l is a lattice vector of the crystal and m is an integer. Therefore each electronic wave function can be written as a sum of plane waves,

$$\psi_i(r) = \sum_G c_{i,k+G} \exp[i(k+G) * r]. \tag{11}$$

The Bloch theorem changes the problem of calculating an infinite number of electronic wave functions to one of calculating a finite number of electronic wave functions at an infinite number of k points. However the electronic wave functions at k points that are

very close together will be almost identical. Hence, it is possible to represent the electronic wave functions over a region of k space by the wave functions at a single k-point. In this case the electronic states at only a finite number of k points are required to calculate the electronic potential and hence determine the total energy of the solid. Methods have been devised for obtaining very accurate approximations to the electronic potentials and the contribution to the total energy from a filled electronic band by calculating the electronic states at special sets of k points [50, 51]. Using these methods, one can obtain an accurate approximation for the electronic potential and the total energy by calculating electronic states at a very small number of k points.

Bloch's theorem states that the electronic wave functions at each k point can be expanded in terms of a discrete plane-wave basis set. In principle, an infinite plane-wave basis set is required to expand the electronic wave functions. However, the coefficients $c_{i,k+G}$ for the plane waves with small kinetic energy $(\hbar^2/2m)|k+G|^2$ are typically more important than those with large kinetic energy. Thus the plane-wave basis can be truncated to include only plane waves that have kinetic energies less than some particular cutoff energy. Introduction of an cutoff energy to the discrete plane-wave basis set produces a finite basis set.

When plane-waves are used as a basis set for the electronic wave functions, the Kohn-Sham equations assume a particularly simple form. Substitution of Eq.(11) into (3) and integration over r gives the secular equation

$$\sum_{G'} \left[\frac{\hbar^2}{2m} |k+G|^2 \delta_{GG'} + V_{ion}(G-G') + + V_H(G-G') + + V_{XC}(G-G') \right] c_{i,k+G'} = \\ = \varepsilon_i \, c_{i,k+G}. \quad (12)$$

In this form, the kinetic energy is diagonal, and the various potentials are described in terms of their Fourier transforms. Solution of Eq. (12) proceeds by diagonalization of a Hamiltonian matrix whose matrix elements $H_{k+G,k+G'}$ are given by the terms in the brackets above. The size of the matrix is determined by the choice of cutoff energy $(\hbar^2/2m)|k+G_c|^2$.

The Bloch theorem can be applied neither to a system that contains a single defect nor in the direction perpendicular to a crystal surface. Calculation using plane-wave basis set can only be performed on these systems if a periodic supercell is used. The supercell contains the defect surrounded by a region of bulk crystal. Periodic boundary

conditions are applied to the supercell so that the supercell is reproduced throughout space. Therefore the energy per unit cell of a crystal containing an array of defects is calculated, rather than the energy of a crystal containing a single defect. It is essential to include enough bulk solid in the supercell to prevent the defects in neighboring cells from interacting with each other.

4.3 Pseudopotential approximation

A plane-wave basis set is usually very poorly suited to expanding electronic wave functions because a very large number of plane waves are needed to expand the tightly bound core orbitals and to follow the rapid oscillations of the wave functions of the valence electrons in the core regions. These oscillations maintain the orthogonality between the core wave functions and the valence wave functions, which is required by the exclusion principle. The pseudopotential approximation [52, 53, 54] allows the electronic wave functions to be expanded using a much smaller number of plane-waves.

It is well known that most physical properties of solids are dependent on the valence electrons to a much greater extent than the core electrons. The pseudopotential approximation exploits this removing the core electrons and by replacing them by a weaker pseudopotential that acts on a set of pseudo wave functions rather than the true valence wave functions. The pseudopotential is constructed ideally, so that its scattering properties or phase shift for the pseudo wave functions are identical to the scattering properties of the ion and the core electrons for the valence wave functions, but in such a way that the pseudo wave functions have no radial nodes in the core region. Outside the core region the two potentials are identical, and the scattering from the two potentials is indistinguishable.

Various groups have now introduced pseudopotentials of many elements that work extremely well [55, 56].

4.4 Computational procedure with matrix diagonalization

The sequence of steps required to carry out a total energy pseudopotential calculation with conventional matrix diagonalization techniques is shown in the flow diagram in Fig. 2. The procedure requires an initial guess for the electronic charge density, from which the Hartree potential and the exchange-correlation potential can be calculated. The Hamiltonian

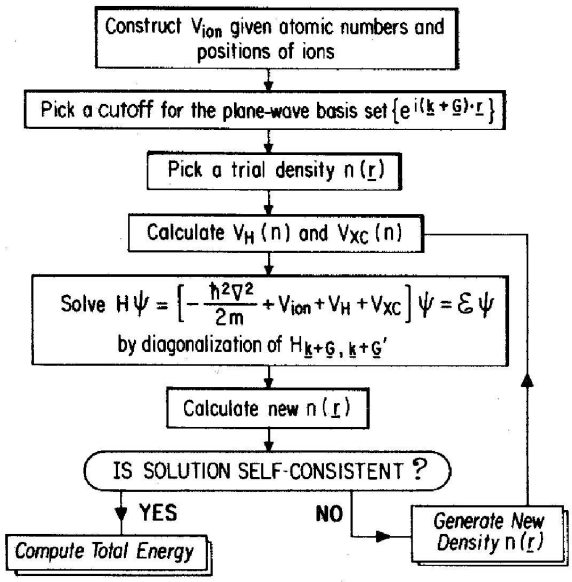

Figure 2: Flow chart describing the computational procedure for the calculation of the total energy of a solid, using conventional matrix diagonalization (taken from [42]).

matrices for each of the k points included in the calculation must be constructed, as in Eq. (12), and diagonalized to obtain the Kohn-Sham eigenstates. These eigenstates will normally generate a different charge density from the one originally used to construct the electronic potentials, and hence a new set of Hamiltonian matrices must be constructed using the new electronic potentials. The eigenstates of the new Hamiltonians are obtained, and the process is repeated until the solutions are self-consistent. To complete the total energy calculations, tests should be performed to ensure that the total energy is converged both as a function of the number of k points and as a function of the cutoff energy for the plane-wave set.

5 Tight-binding model

Tight-binding molecular dynamics is a useful method for studying the structural, dynamical, and electronic properties of covalent systems. The method incorporates electronic structure calculation into molecular dynamics through an empirical tight-binding Hamiltonian and bridges the gap between *ab initio* molecular dynamics and simulations using empirical classical potentials.

5.1 The bond energy model

The tight binding model has been developed on the basis of two major approximations. The first to be considered is the adiabatic approximation [43], which is based on the fact that electrons move typically $\sim 10^2 - 10^3$ faster than the ions. The latter can thus be considered in their ground state at any moment for a particular instantaneous ionic configuration, and the electronic and ionic degrees of freedom can therefore be separated. The second approximation consists in reducing the N-body problem to a one-electron scheme, where each electron moves independently of the others, and experiences an effective interaction due to the other electrons and to the ions. Within these approximations, the one-particle electronic part of the total Hamiltonian can be written in the form

$$\hat{H} = \hat{T}_e + \hat{U}_{ee} + \hat{U}_{ei}, \tag{13}$$

where $\hat{T}_e$ is the kinetic energy operator of the electrons, $\hat{U}_{ee}$ and $\hat{U}_{ei}$ are the electron-electron and electron-ion interactions respectively. Following the notation of Horsfield *et. al.* [59], the single-particle Schrödinger equation is

$$\hat{H}|n\rangle = \epsilon^{(n)}|n\rangle, \tag{14}$$

where $|n\rangle$ is a single particle (doubly occupied) eigenfunction, and $\epsilon^{(n)}$ is the corresponding eigenvalue. It has to be mentioned that the $\mathbf{k}$ dependency of $|n\rangle$ and $\epsilon^{(n)}$ does not appears explicitly in the notation for clarity. The eigenfunctions are expanded in an atomiclike (Löwdin) orbitals set [57]

$$|n\rangle = \sum_{i\alpha} C_{i\alpha}^{(n)}|i\alpha\rangle \tag{15}$$

where i is a site index and α an orbital index. It has to be noted that the basis used to expand the wave functions may be non-orthogonal. However, in the present work,

orthogonal basis functions are used. The influence of this choice on the results will be discussed further.

Taking into account the orthonormality of the eigenstates, the eigenvalues and eigenstates of the Hamiltonian are therefore found by solving the matrix equation

$$\sum_{j\beta} H_{i\alpha,j\beta} C_{j\beta}^{(n)} = \epsilon^{(n)} C_{i\alpha}^{(n)}, \tag{16}$$

where

$$H_{i\alpha,j\beta} = \langle i\alpha|\hat{H}|j\beta\rangle \tag{17}$$

are the matrix elements and

$$\sum_{i\alpha} C_{i\alpha}^{(n)} C_{i\alpha}^{(m)} \equiv \sum_{i\alpha} \langle n|i\alpha\rangle\langle i\alpha|m\rangle = \delta_{n,m}. \tag{18}$$

The off-diagonal matrix elements $H_{i\alpha,j\beta} = \langle i\alpha|\hat{H}|j\beta\rangle$, for $i\alpha \neq j\beta$, are called *hopping integrals*, and the on-site elements $H_{i\alpha,i\alpha}$ are the atomic orbital energies. In the tight binding approach, these hopping integrals and the on-site matrix elements are constants to be fitted on the basis of the following approximations:

(i) Only atomic orbitals whose energy is close to that of the energy bands on is interested in, are used [58]. This is the *minimal basis set* approximation. Thus, for instance, only the $2s$ (one orbital) and $2p$ (three orbitals: p_x, p_y, and p_z) orbitals are considered in the case of diamond and $3s$ and $3p$ orbitals for silicon, to describe the occupied (valance) bands. For these two materials there are 16 possible hopping integrals. However, it can be shown [60] that only hopping integrals between orbitals with the same angular momentum about the bond axis, are non-vanishing. There remain therefore just four nonzero hopping integrals, labeled $(ss\sigma)$, $(sp\sigma)$, $(pp\sigma)$, and $(pp\pi)$. σ stands for orbitals with 0 angular momentum about the bond axis and π for orbitals with angular momentum $\pm$ 1. The dependence of these hopping integral in the distance between the atoms will be considered further.

(ii) One considers only hopping integrals between two atoms separated by a distance shorter than a suitable cutoff. Obviously, to reduce the number of parameters to be fitted, a cutoff which includes the nearest neighbors is appropriate. However, the orthogonalized functions (Löwdin) extend further than those (non-orthogonal) from which they are derived, because the orthogonalization procedure involves orbitals from nearby atoms.

Thus, interactions extending beyond first nearest neighbors have to be taken into account when an orthogonal basis is used.

Considering the approximations above, the off-diagonal elements of the Hamiltonian matrix $H_{i\alpha,j\beta} = \langle i\alpha|\hat{H}|j\beta\rangle$ (for $i\alpha \neq j\beta$) are fitted to electronic band structure of the equilibrium crystal phase, as calculated by more accurate first-principle models [61]. Sets of hopping integrals can thus be obtained for each crystalline structure considered.

The tight-binding expression for the binding energy of a system with N atoms [63] is given by :

$$E_{binding} = E_{bs} + E_{rep} = 2 \sum_{n(occ.)} \epsilon^{(n)} + E_{\rm rep} \tag{19}$$

where $E_{\rm bs}$ is the band energy and $E_{\rm rep}$ is the repulsive potential, given as a sum of pair potentials. $\epsilon^{(n)}$ are the eigenvalues obtained from the diagonalization of the Hamiltonian matrix. Within the adiabatic approximation, the electrons are assumed to be in their ground state, so that all the states below the Fermi level are occupied, and the summation that appears in the band energy is made over these occupied $\mathbf{k}$ states. $E_{\rm rep}$ accounts for the ion-ion repulsion, for the double counting of electron-electron interactions that appears in the band energy, for the repulsion of overlapping orbitals due to Pauli's principle and for the exchange-correlation energy related to the N-body electronic interaction. The form of the repulsive energy $E_{\rm rep}$ proposed by Xu *et. al.* [63] and used in the present research is

$$E_{\rm rep} = \sum_i f\left(\sum_j \phi(r_{ij})\right), \tag{20}$$

where f is a functional expressed as a 4th-order polynomial, $\phi(r)$ is a pairwise potential between atom i and atom j, and described below, and r_{ij} is the interatomic distance between the atoms.

5.2 The rescaling functions

As mentioned above, the elements of the Hamiltonian matrix are fitted to first-principle calculations for different equilibrium structures [61]. To describe the properties of non-equilibrium structures, as amorphous solids or liquids, the hopping integrals and the repulsive energy should be rescaled with respect to the interatomic distance. The rescaling functions proposed by Goodwin *et. al.* [62] greatly improve the transferability of the tight

binding model to structures not included in the parameterization. These functions are now widely used, in the slightly improved form proposed by Xu *et. al.* [63]

$$h(r) = h_0(r_0/r)^n \exp\{n[-(r/r_c)^{n_c} + (r_0/r_c)^{n_c}]\}, \tag{21}$$

for the rescaling of the hopping integrals, and

$$\phi(r) = \phi_0(d_0/r)^m \exp\{m[-(r/d_c)^{m_c} + (d_0/d_c)^{m_c}]\} \tag{22}$$

for the repulsive potential. In the rescaling functions found by Goodwin em et. al., the parameters n_c and r_c were the same as m_c and d_c respectively. All the parameters appearing in the rescaling functions are obtained by fitting first principle results of energy versus nearest-neighbor interatomic distance for different crystalline phases, given equilibrium sets of hopping integrals for these structures. In this way, the tight binding model is transferable to different atomic environments.

6 Numerical techniques

6.1 Force calculation

We can express the forces acting on the atoms in a compact form, by first defining the density matrix

$$\rho_{i\alpha,j\beta} = \sum_{n(occ.)} C_{i\alpha}^{(n)} C_{j\beta}^{(n)} \tag{23}$$

The cohesive energy thus becomes

$$E_{\rm tot} = 2 \sum_{i\alpha,j\beta} \rho_{j\beta,i\alpha} H_{i\alpha,j\beta} + U_{\rm rep} \tag{24}$$

The forces acting on the atoms are then obtained by differentiating the cohesive energy with respect to atomic positions, that is

$$\mathbf{F}_k = -\frac{\partial E_{\rm tot}}{\partial \mathbf{r}_k} \tag{25}$$

$$= -\left\{ 2 \sum_{i\alpha,j\beta} \rho_{j\beta,i\alpha} \frac{\partial H_{i\alpha,j\beta}}{\partial \mathbf{r}_k} + \frac{\partial U_{\rm rep}}{\partial \mathbf{r}_k} \right\}. \tag{26}$$

6.2 Equations of motion

Once the forces which act on each atom i are calculated, we solve the differential equations:

$$f_{\alpha i} = m \frac{d^2 R_{\alpha i}}{dt^2} = -\frac{\partial E}{\partial R_{\alpha i}} \tag{27}$$

$$v_{\alpha i} = \frac{dR_{\alpha i}}{dt} \tag{28}$$

in order to obtain the position R_i and the velocity v_I of each atom of mass m as a function of the time t. I is the atom in consideration and α the coordinates x, y and z. In order to solve the Newton's equations (27) and (28) for coordinates x, y and z and velocities v_x, v_y and v_z, the algorithm Verlet was used.

6.3 The Verlet algorithm

To derive the Verlet algorithm, we start with a Taylor expansion of the coordinate of a particle, around time t,

$$r(t+\Delta t) = r(t) + v(t)\Delta t + \frac{f(t)}{2m}\Delta t^2 + \frac{\Delta t^3}{3!}\dddot{r} + O(\Delta t^4), \tag{29}$$

similarly,

$$r(t-\Delta t) = r(t) - v(t)\Delta t + \frac{f(t)}{2m}\Delta t^2 - \frac{\Delta t^3}{3!}\dddot{r} + O(\Delta t^4). \tag{30}$$

Summing these two equation, we obtain:

$$r(t+\Delta t) + r(t-\Delta t) = 2r(t) + \frac{f(t)}{m}\Delta t^2 + O(\Delta t^4) \tag{31}$$

or

$$r(t+\Delta t) \approx 2r(t) - r(t-\Delta t) + \frac{f(t)}{m}\Delta t^2. \tag{32}$$

One can derive the velocity from knowledge of the trajectory:

$$v(t) = \frac{r(t+\Delta t) + r(t-\Delta t)}{2\Delta t} + O(\Delta t^2). \tag{33}$$

6.4 General description of the calculations

The Oxford Order N (OXON) [64] package is one of those that will used in the present project. This is a set of programs for carrying out atomistic static and dynamic calculations using potentials which are based on tight-binding methods.

The tight-binding method will be employed in the calculations to describe interactions between carbon atoms. With this method, the molecular dynamics technique will be applied to calculate the positions and the velocities of the atoms as function of the time. In the MD calculation, Newton's equations of motion will be solved using the Verlet algorithm. The MD time step will 0.5×10^{-15} s. Periodic boundaries conditions will applied to the sample.

The ABINIT code [65] will be used to calculate the exact electronic structure of obtained samples. ABINIT is a package which allows to find the total energy, charge density and electronic structure of systems made of electrons and nuclei (molecules and periodic solids) using *ab initio* approximations described in section 4 with many pseudopotential types. The code carries out automatic k-point sampling of the irreducible Brilliouin zone.

In order to calculate the ratio of sp^2 to sp^3 bonded atoms, as well as the radial and angle distribution functions of the structures of amorphous carbon generated a FORTRAN program was written.

6.5 AViz

Our computational physics group developed the Atomic Vizualization package **AViz** [66]. This is very powerful vizualization tool which helps to enhance 3D perception. It includes various options which let one to rotate the still sample, change relative sizes of atoms, create animations and movies, add and remove the bonds and borders of the sample, use color coding, slice the sample and much more.

The Atomic Vizualization package **AViz** will be used in all stages of this work. A vizualization of our nanodiamond samples with color coding for different atomic bonding will help to clarify the structure of amorphous envelope and boundary region between diamond and amorphous carbon. It will be essential for understanding how the these regions affect quantum confinement effects.

7 Preliminary results

7.1 Test of *ab initio* code

The OXON code was used extensively in [19], so we do not need to test it here. Another code, which we will use in this project, is the ABINIT code. This is an accurate tool to measure electronic properties of our samples. This code requires very carefull choosing of the pseudopotential for carbon, its cutoff energy and k-point sampling. The choise should be adjusted in well-known situation. In order to check the reliability of the ABINIT code [65] based on density functional theory within local-density approximation a calculation of the location of hydrogen in diamond was carried out and results was compared with previous calculations [67]. The nonlocal norm-conserving pseudopotential of Troullier-Martin [55] was used in these simulations. With this choice of pseudopotential, the kinetic energy cutoff of up to 30 Ry lead to good convergence with respect to plane-wave basis. Perfect diamond cubic cells with diameter from 3.55×3.55×3.55 Å (8 atoms) to 7.1×7.1×7.1 Å (64 atoms) was used, and a 2×2×2 Monkhorst-Pack **k**-point mesh [51] was employed.

According to [67] the most important interstitial sites of hydrogen in the diamond structure are: the T-site which lies equidistant from four carbon sites and possesses T_d symmetry, the H-site which lies midway between two T-sites and possesses D_{3d} symmetry and the bond-centered (BC) site is the mid-point between two carbon atom site (D_{3d} symmetry).

To confirm this simulations were carried out at 0 K. An atom of hydrogen was placed at different positions inside a diamond lattice. In each step the interatomic forces were computed, and the atoms were moved in the force gradient directions. The simulation will stop if the forces are below some value selected as the stopping criterion.

In the cases where the hydrogen atom was placed in a position located on the line connecting two carbon atoms (independently of the distance from the carbon atoms) or on a line perpendicular the C-C bond (which cross the bond midway with an angle between this C-C bond and C-H bond were up to 15°) the hydrogen atom transferred to the BC-site (see Fig. 3). The diamond lattice was distorted, the carbon atoms neighboring to a hydrogen atom being pushed apart such that the C-C distance was larger than in diamond (1.54 A). The C-H bond length and the new C-C distance were measured and have been found to be in excellent agreement with an *ab initio* calculations of Goss [67]

C-H distance Å	C-C dilation (%)	Method
1.13	52	Tight-binding 64-atom supercell [68]
1.17	47	*Ab initio* (LDA-DFT) 64-atom supercell [67]
1.17	47	present simulations, 8 and 64-atom supercells

Table 1: Properties of BC position of hydrogen in diamond

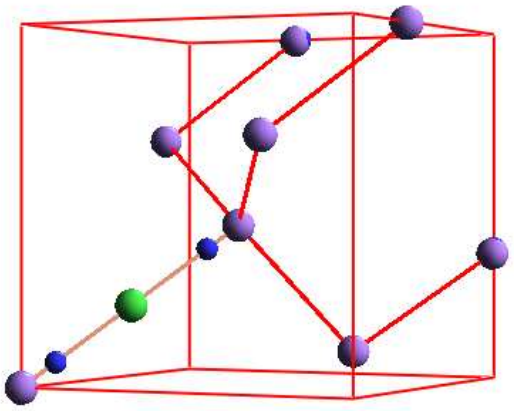

Figure 3: BC-site of hydrogen atom in diamond, green atom is a hydrogen, violet atoms are carbon, small blue atoms represent undistorted diamond lattice.
[h]

(see Tab. 1).

In most of cases, calculations of the location of hydrogen in diamond initially placed in a random position have led it to T-site (see Fig. 4). In the T-site a hydrogen atom is located at a distance of 1.55 Å from neighboring carbon atoms, this is very close to diamond bond length (1.54 Å). The potential well of the H-site was found to be very narrow. Only hydrogen atoms which initially have been placed exactly at the H-site, have not escape from there (see Fig. 5). The energies of hydrogen in the various sites in diamond varies considerably, for example BC-site have lowest energy. Table below 2 lists the relative energies of hydrogen at the H, T and BC-sites (in eV).

A new hydrogen site was found at finite temperatures by D. Saada et al. [68] and confirmed by O. Hershkovitz [38] using tight-binding techniques. This structure was

BC	T	H	Method
0.0	0.5	-	Tight-binding 64-atom supercell [68]
0.0	1.0	1.7	*Ab initio* (LDA-DFT) 64-atom supercell [67]
0.0	1.16	1.94	*Ab initio* (LDA-DFT) [69]
0.0	1.17	1.79	present simulations, 8-atom cell

Table 2: Relative energies of different positions of hydrogen in diamond

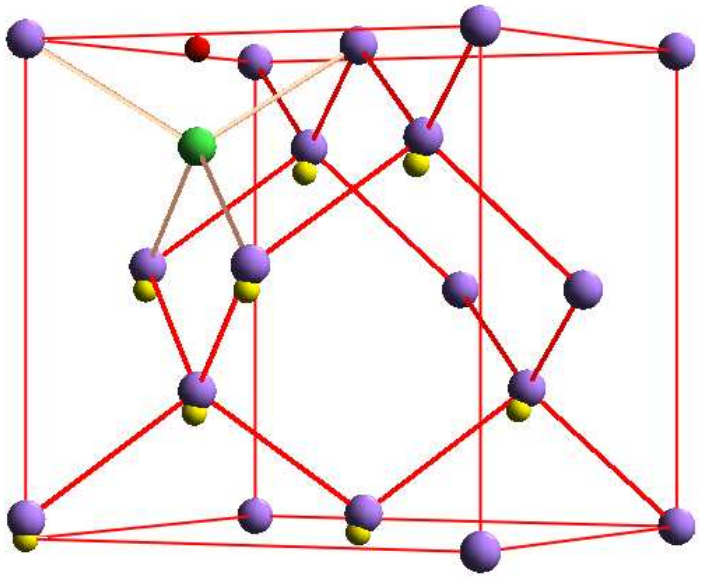

Figure 4: T-site of hydrogen atom in diamond, green atom is a hydrogen, violet atoms are carbon, yellow atoms represent undistorted diamond lattice atoms and the initial position of the hydrogen is shown by red ball.

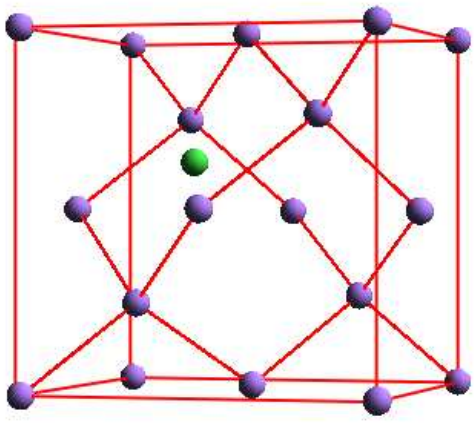

Figure 5: H-site of hydrogen atom in diamond, green atom is a hydrogen, violet atoms are carbon.

labelled equilateral triangle (ET) due to the two sets of three equivalent sites around the C-C bond that the H atom could adopt. The length of C-H bond is 1.08 A, that is closer than BC site. The ET-site was predicted to be 1.4 eV lower in energy than the BC-site. However, *ab-initio* calculations of Goss [67] and the present calculations carried out at at 0 K shows that this site is unstable: hydrogen atoms initially placed in the ET-site have migrated to BC-site (see Fig.6).

These results are in good agreement with previous calculations of Goss [67], so the ABINIT code with the Troullier-Martin pseudopotential and chosen cutoff energy may become an appropriate instrument for further calculations to resolve this issue.

7.2 Geometry and preparation of nanodiamonds structures

7.2.1 Nanodiamond layers inside amorphous carbon phase

Nanodiamond sheets surrounded by amorphous carbon sheets were generated and described in the Msc thesis of Anastassia Sorkin. Three different unit cells with a density of 3.5 g/cc, initially arranged as a perfect diamond crystal, were constructed, their sizes are 2 × 2 × 6 (192 atoms), 2 × 2 × 7 (224 atoms) and 2 × 2 × 8 (256 atoms). The 32 upper and 32 lower atoms of each sample were frozen, i.e. the motion of these atoms

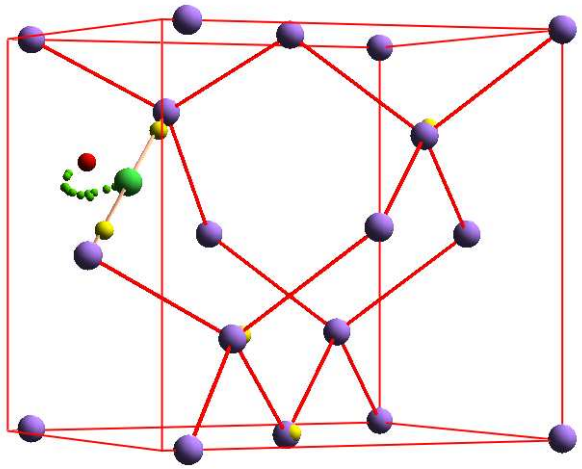

Figure 6: Migration (small green balls) of hydrogen atom from ET to BC-site, green atom is a hydrogen, violet atoms are carbon, yellow atoms represent undistorted diamond lattice, initial ET position of hydrogen is shown by red ball.

was forbidden. The remaining central layers were heated up to temperatures of 14000-30000 K. Once the hot liquid layers reached equilibrium, the central layers were cooled to the room temperature of 300 K by a cooling rate of 10 K/fs. After cooling the hot layers remained partially or entirely amorphous with the presence of three- and two- fold coordinated atoms in the structure. By this way the structures of amorphous carbon located between two layers of diamond of 32 atoms each were constructed. With periodic boundary conditions this sample can be imagined as diamond layers surrounded by two layers of amorphous carbon see Fig. 7. The thickness of this diamond frozen layer in all three samples was 7.1 Å (32 + 32 =64 atoms), and the thickness of the hot layers varied from 7.1 (64 atoms) to 10.65 Å (96 atoms) for these three samples.

Moreover it turned out that the volume of the region, which returns to diamond as well as a volume of remaining amorphous region and sp^2/sp^3 ratio in this amorphous region strongly depended on the temperature of heating and the thickness of the hot layers [19]. It means that that a size of our diamond nanolayers can be changed not only by simple increasing of frozen diamond layers, but by increasing of heating temperature. If the heating temperature was too low (depending on thickness of the hot layers), the amorphous region were too thin (thinner than 3.5 Å, that is cutoff radius of interaction between carbon atoms), and diamond layers could interact across this amorphous region (for example see Fig.8). Such a samples were discarded from further calculations.

The structures were found to be very stable during further relaxation at a temperatures up to 10000 K during 3 ps. The structural and electronic properties of each sample were studied. The sp^2/sp^3 coordinated atoms ratio, thickness of diamond layer and band gap of each sample calculated by tight-binding method are represented in Table 3 below. The results do not show quantum confinement effects, i.e. the band gap of the whole sample does not increase with decreasing of the thickness of the diamond layer, even for the samples with the same value of the sp^2/sp^3 ratio. It can be explained by the fact, that thickness of outer amorphous layers in these samples is different, and electronic properties of the sample depend not only on quantum confinement and the sp^2/sp^3 ratio, but on thickness of amorphous layers and individual configuration of each sample.

7.2.2 Nanodiamond cluster surrounded by amorphous phase

The sample of diamond cluster surrounded by amorphous carbon (see Fig.9) was generated by O. Hershkovitz and forwarded to us for further studies. This sample contain 512

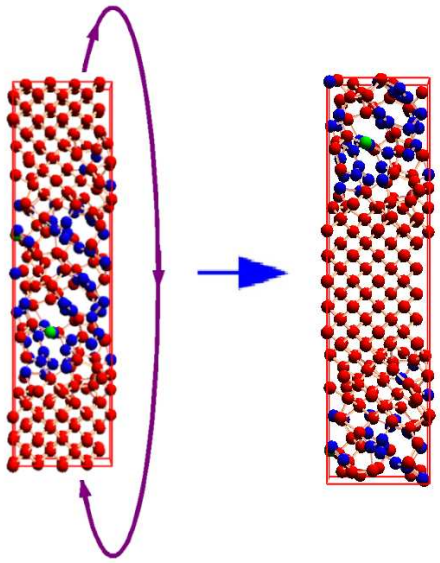

Figure 7: The sample of amorphous carbon located between two layers of diamond (left) and the same sample imagined as diamond located between two layers of amorphous carbon (right). The sample contain 256 atoms (64 of them are frozen diamond), temperature of heating was 23000 K. Red balls represent fourfold coordinated atoms, blue balls represent threefold coordinated atoms, green balls represent twofold coordinated atoms.

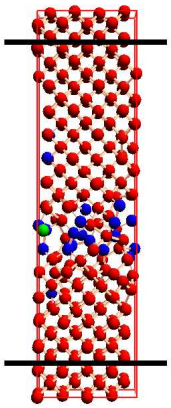

Figure 8: The sample of amorphous carbon located between two layers of diamond which is not suitable for further calculations. The sample contain 256 atoms (64 of them are frozen diamond). The frozen outer layers are separated by black line. After cooling from 16000 K, most part of the hot layer returned to diamond, and only a layer of thickness of 3 Å remained amorphous. Red balls represent fourfold coordinated atoms, blue balls represent threefold coordinated atoms, green balls represent twofold coordinated atoms.

Number of hot layers in diamond unit cells	Temperature of heating	sp^2/sp^3 ratio in the hot layers after cooling	Thickness of diamond layer (Å)	Band gap (eV)
4	23000 K	0.26	14.2	1,7
4	28000 K	0.34	12.4	1.3
4	30000 K	0.6	12.4	1
5	20000 K	0.27	16.56	2
5	23000 K	0.4	12.4	0.4
6	17000 K	0.26	23.6	3
6	20000 K	0.35	16.56	2.3
6	23000 K	0.45	9.4	0.9

Table 3: The sp^2/sp^3 coordinated atoms ratio, thickness of diamond layer and a band gap of samples generated in this section

carbon atoms (4×4×4 diamond unit cells) at density of 3.55 g/cc. Initially, atoms were arranged as perfect diamond. Then an inner cubic cluster of size 2×2×2 diamond unit cells (7.1×7.1×7.1) was frozen, i.e. the motion of atoms in the cluster was forbidden. The remaining outer envelope was heated up to 35000 K, all attempts to obtain disordered liquid phase at lower temperatures failed. Once the liquid phase reached equilibrium, the temperature was immediately decreased to room temperature. The system remained stable during further simulations at 300 K (2 ps), however additional structural relaxation is required. The percentage of sp^2 and sp^3 coordinated atoms before a relaxation was calculated as 73 and 27% respectively.

7.2.3 Other possible geometries

The third type of nanodiamond structure which will be studied in this project is a sample of diamond nanowires surrounded by amorphous carbon. Detailed conditions of their creation (such as heating temperature and cooling rate) are yet not clear. It may by supposed that temperature of heating will higher than in the case of nanodiamond layers but lower than in the case of clusters.

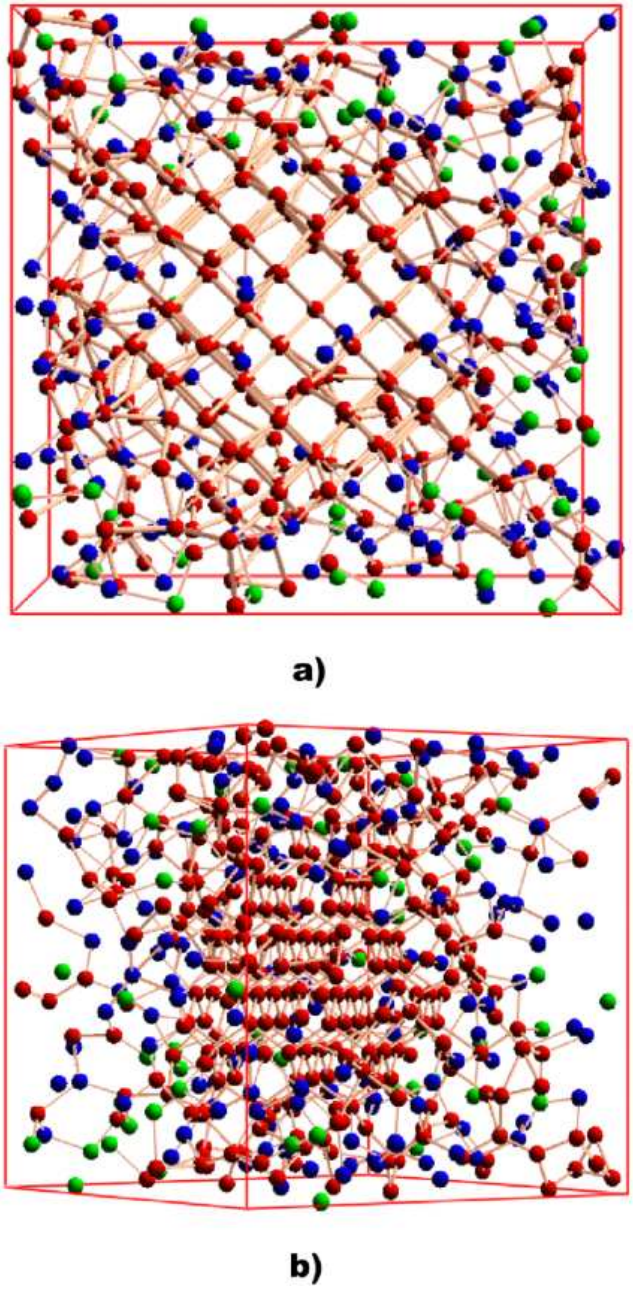

Figure 9: The diamond cluster surrounded by amorphous carbon phase (the sample was built by O. Hershkovitz): a) view from $< 001 >$ direction, b) view from $< 210 >$ direction. Red balls represent fourfold coordinated atoms, blue balls represent threefold coordinated atoms, green balls represent twofold coordinated atoms.

8 Workplan

1. In the first stage of the research the ABINIT code with the Troullier-Martin pseudopotential and the local-density approximation was tested for convergence in order to choose a suitable cutoff energy for plane-waves as well as a suitable number of k-points. Some additional comparisons with known theoretical results (for example calculation of location and energy of hydrogen within diamond lattice) were made.

2. The next part of the calculations will be focused on the conditions of sample preparation by tight-binding molecular dynamics.

   (a) The diamond layers sandwiched between two layers of amorphous carbon will be generated as described in subsection 7.2.1. The samples with different thickness of diamond layers can be obtained not only by simply increasing of number of atoms in the system, but by variation of the temperature of heating. The samples can contain a different fraction of sp^2 and sp^3 coordinated atoms in the outer amorphous layers.

   (b) In order to generate diamond nanoclusters inside an amorphous carbon phase, an outer region of perfect diamond samples of different thicknesses will be heated up to 35000 K (which is higher than in the case of diamond layers) and then quenched (see subsection 7.2.2). The inner cluster of perfect diamond will remain frozen. The simulations will be carried out at different temperatures and different sizes of the hot envelope.

   (c) In order to generate diamond nanowires, i.e. a nanodiamond tube inside an amorphous carbon phase, a small region with the form of tube inside a perfect diamond sample will be frozen, and the outer envelope will be heated and quenched as described in the previous item. The simulations will be carried out at different temperatures. Wires of different diameter (from 3.55 Å and larger) will be generated.

   In this way nanodiamond of different sizes surrounded by amorphous phase of different structure (percentage of sp^2 and sp^3 coordinated atoms) will be created. Structural relaxation of each sample will be carried out by the *ab initio* method.

3. The structural properties of each sample (RDF, density profile, percentage of sp^2 and sp^3 in amorphous envelope) will be calculated by the FORTRAN programs, which were already written in [19]. Electronic properties of each sample will be obtained as part of the tight-binding and *ab initio* calculations.

4. Quantum confinement effects, i.e. the dependence of band gap (higher occupied and lower unoccupied energetic state) on sizes of nanodiamonds will be researched for different dimensions of the nanodiamond structures (from zero for clusters to two for layers). Additional factors which can influence the results (for example, history of sample preparation, structure of amorphous envelope) will be established.

References

[1] Y. K. Chang, H. H. Hsieh, W. P. Pong, M. H. Tsai, F. H. Chien, P. K. Tseng *et al.*, Phys. Rev. Letters, **82**, 5377 (1999)

[2] A. I. Ekimov, A. A. Onushchenko, Sov. Phys. Semicond. **16**, 775 (1982)

[3] E. Corcoran, Sci. Am., 263 (November), 74 (1990)

[4] Y. Maeda, N. Tsukamoto, Y. Yazawa, Y. Kanemitsu, Y. Masumoto, Appl. Phys. Lett., **59**, 2187 (1992)

[5] E. W. Draeger, J. C. Grossman, A. J. Williamson, G. Galli, Phys. Rev. Lett, **90**, 167402 (2003)

[6] A. Puzder, A. J. Williamson, J. C. Grossman, G. Galli, Phys. Rev. Lett, **88**, 097401 (2002)

[7] R. Rosetti, S. Nakahara, J. E. Brus, J. Phys. Chem., **79**, 1086 (1983)

[8] M. V. Rama Krishna, R. A. Friesner, J. Phys. Chem., **95**, 8309 (1991); **105**, 3612 (1996)

[9] K. E. Andersen, C. Y. Fong, W. E. Pickett, J. Non-Cryst. Sol., **299-302**, 1105 (2002)

[10] S. Öğut, J. R. Chelikowsky, Phys. Rev. Lett, **79**, 1770 (1997)

[11] P. Badziag, W. S. Verwoerd, W. P. Ellis, N. R. Greiner Nature, **343**, 244 (1990)

[12] R. S. Lewis, M. Tang, J. F. Wecker, E. Anders, E. Steel, Nature, **326**, 160 (1987)

[13] R. S. Lewis, E. Anders, B. T. Draine,, Nature, **339**, 117 (1989)

[14] N. R. Greiner, D. S. Phillips, J. D. Johnson, A. F. Volk, Nature, **333**, 440 (1989)

[15] J. Y. Raty, G. Galli, C. Bostedt, T. W. van Buuren, L. J. Terminello, Phys. Rev. Letters, **90**, 037401 (2003)

[16] http://www.nanodiamond.com/

[17] L. Pauling, *The Nature of the Chemical Bond*, Cornell University press, (1948)

[18] F. P. Bundy, Physica A, **156**, 169 (1989)

[19] A. Sorkin *Computational study of structures of diamond and amorphous carbon under extreme heating and cooling*, M.Sc.thesis, Technion (2003)

[20] W. D. Callister Jr. *Material Science ang Engeneering*

[21] B. Hettich, http://www.ornl.gov/info/ornlreview/rev26-2/text/rndmain1.html

[22] A.Heiman, I.Gouzman, S.H. Christiansen, H.P.Strunk, G.Comtet, L.Hellner, G.Dujardin, R.Endrei, A.Hoffman, J. Appl. Phys. **89**, 2622 (2001)

[23] http://www.eng.rpi.edu/dept/materials/COURSES/NANO/oja/

[24] J. E. Brus, J. Phys. Chem., **79**, 5566 (1983); **80**, 4403 (1984)

[25] P. E. Batson, J. E. Heath, Phys. Rev. Lett., **71**, 911 (1993)

[26] R. E. Hummel, *Electronic Properties of Materials*, Springer-Verlag, Berlin (1994)

[27] P. E. Lippens, M. Lanoo, Phys. Rev. B, **39**, 10935 (1989)

[28] L. T. Canham, Appl. Phys. Lett., **57**, 1046 (1990)

[29] J. B. Xia, K. W. Cheah, J. Phys. Condens. Matter, **9**, 9853 (1997)

[30] C. Y. Yeh, S. B. Zhang, A. Zunger, Phys. Rev. B, **50**, 14405 (1994)

[31] Y. M. Niquet, C. Delerue, G. Allan, M. Lanoo, Phys. Rev. B, **62**, 5109 (2000)

[32] Y. M. Niquet, C. Delerue, G. Allan, M. Lanoo, Appl. Phys. Lett., **77**, 1182 (2000)

[33] G. Allan, C. Delerue, M. Lanoo, Appl. Phys. Lett., **71**, 1189 (1997)

[34] B. Delley, E. F. Steigmeier, Phys. Rev. B, **47**, 1397 (1997)

[35] F. Buda, J. Kohanoff, M. Parinello, Phys. Rev. Lett, **69**, 1272 (1992)

[36] M. G. Fyta, I. N. Remediakis, P. C. Kelires, Phys. Rev. B, **67**, 035423 (2003)

[37] Y. Lifshitz, Th. Köhler, Th. Frauenheim, I. Guzmann, A. Hoffman, R. Zhang, X. Zhou, S. Lee, Science, **297**, 1531 (2002)

[38] O. Hershkovitz, M.Sc.thesis, Technion (2004), http://www.technion.ac.il/ orenh/

[39] B.L. Zhang, C.H. Xu, C.Z. Wang, C.T.Chan, K.M.Ho, Phys.Rev.B **46**, 7333 (1992)

[40] C.Z. Wang, K.M. Ho, C.T. Chan, Phys. Rev. Lett. **70**, 611 (1993)

[41] C.Z. Wang, K.M. Ho, Phys. Rev. Lett. **71**, 1184 (1993)

[42] M. C. Payne, M. P. Teter, D. C. Allan, T. A. Arias, J. D. Joannopoulos, Rev. Modern Phys, **64**, 1045 (1992)

[43] M. Born, J. R. Oppenheimer, Ann. Phys. **84**, 457 (1927)

[44] P. Hohenberg, W. Kohn, Phys. Rev. **136**, 864B (1964)

[45] W. Kohn, L. J. Sham, Phys. Rev. **140**, 1133A (1965)

[46] E. P. Wigner, Trans. Faraday Soc. **34**, 678 (1938)

[47] L. Hedin, B. Lundqvist, J. Phys. C **4**, 2064 (1971)

[48] J. P. Perdew, A. Zunger, Phys. Rev. B **23**, 5048 (1981)

[49] C. Kittel, *Introduction to Solid State Physics* (1986)

[50] D. J. Chadi, M. L. Cohen, Phys. Rev. B **8**, 5747 (1973)

[51] H. J. Monkhorst, J. D. Pack, Phys. Rev. B **13**, 5188 (1976)

[52] J. C. Phillips, Phys. Rev. **112**, 685 (1958)

[53] M. L. Cohen, V. Heine, Sol. State Phys., **24**, 37 (1970)

[54] M. T. Yin, M. L. Cohen, Phys. Rev. B **25**, 7403 (1982)

[55] N. Trouillier, J. L. Martins, Phys. Rev. B **43** (1991)

[56] D. Vanderbilt, Phys. Rev. B **41**, 7892 (1990)

[57] P.Löwding, J.Chem.Phys. **18**,365 (1950).

[58] J.S.Slater, G.F.Koster, Phys.Rev.B **94**, 1498 (1954)

[59] A.P.Horsfield, A.P.Bratkovsky, M.Fearn, D.G.Pettifor, M.Aoki, Phys.Rev.B **53**, 12694 (1996)

[60] A.P.Sutton, *Electronic Structure of Materials,* (Oxford University Press, 1993)

[61] S.Fahy, S.G.Louie, Phys.Rev.B **36**, 3373 (1987)

[62] L. Goodwin, A.J. Skinner, D.G. Pettifor, Europhys. Lett. **9**, 701 (1989)

[63] C.H. Xu, C.Z. Wang, C.T. Chan, K.M. Ho, J. Phys. Cond. Matt. **4**, 6047 (1992)

[64] andrew.horsfield@materials.ox.ac.uk

[65] http://www.abinit.org/

[66] J. Adler, A. Hashibon, N. Schreiber, A. Sorkin, S. Sorkin and G. Wagner, Computer Physics Communications, **147**, 665-9 (2002)

[67] J. P. Goss, J. Phys. Condens. Matter, **15**, R551 (2003)

[68] D. Saada, J. Adler, R. Kalish, Phys. Rev. B, **61**, 10711 (2000)

[69] J.P.Goss, R. Jones, M. I. Heggie, C. P. Ewels, P. R. Briddon, S. Öberg, Phys. Status Solidi A, **186**, 263)